Two-zone Hall thruster breathing mode mechanism, Part II: Experiment

IEPC-2019-352

Presented at the 36th International Electric Propulsion Conference
University of Vienna, Austria
September 15–20, 2019

Ethan T. Dale* and Benjamin A. Jorns†
University of Michigan, Ann Arbor, MI 48109

A new hypothesis for the Hall thruster breathing mode, in which near-anode and downstream ionization instabilities couple, is experimentally explored. A physically accurate model of this low-frequency instability is desired to better understand Hall thruster performance and stability as a whole. Existing models incompletely or controvertibly describe the breathing mode, and a new "two-zone" mechanism presented in Part I of this study has yet to be validated experimentally. Time-resolved laser and electrostatic diagnostic techniques are used to characterize the internal and near-field plasma and neutral properties in a thruster operated in an oscillatory condition. The phase information of these measurements provided estimates of the electron velocity near the anode – 5.7-11.6 km/s – and density phase lags for neutrals and ions – 142° and 6.5°, respectively. Additionally, an analysis of the data using moments of the Boltzmann equation yields the various steady-state parameters needed to evaluate the two-zone model. Using these data, the model predicts a real frequency and growth rate both near 13 kHz. Although this is slightly lower than the observed frequency of 16 kHz, the closeness still suggests that the model may be capturing the growth of the breathing mode more accurately than existing descriptions like the traditional predator-prey process.

*Ph.D Candidate, Department of Aerospace Engineering, etdale@umich.edu
†Assistant Professor, Department of Aerospace Engineering

Nomenclature

c = speed of light in vacuum, m/s
e = fundamental charge, C
I_d = discharge current, A
L = characteristic length scale, m
n = plasma density, m^{-3}
n_a = plasma density, m^{-3}
n_n = neutral density, m^{-3}
$n_{n,0}$ = injected neutral density, m^{-3}
$n_{n,a}$ = near-anode neutral density, m^{-3}
u_i = ion velocity, m/s
u_e = electron velocity, m/s
$u_{e,a}$ = near-anode electron velocity, m/s
u_n = neutral velocity, m/s
γ = growth rate, rad/s
λ = wavelength, m
λ_0 = nominal wavelength, m
λ_D = Debye length, m
θ = phase angle, deg.
ξ = ionization rate coefficient, m^3/s
ω = frequency, rad/s

I. Introduction

HAll thrusters are a mature in-space propulsion technology that utilize crossed electric and magnetic fields to produce and accelerate a plasma. The high specific impulse and moderate thrust of these devices makes they particularly attractive for near-Earth applications,[1] but gradually they are being slated for deep space missions as well.[2] As this technology is more widely deployed, the reliability of Hall thrusters – not only between ground testing and in-space operation but over their service life as well – becomes increasingly critical.

However, there are several aspects to the operation of Hall thrusters that are still poorly understood, and some of them directly impact their reliability. One example is the "breathing mode": large-amplitude low-frequency oscillations in discharge current. Although this instability has been observed for decades, there is still no definitive analytical criteria for its onset and growth. As a result, the stability of new thrusters cannot be easily predicted in the design phase, and the impact on stability of the ground-to-space transition is unclear. Many hypotheses have been put forward to explain the breathing mode, but due to the inaccessibility of the thruster channel to common diagnostic techniques, little validation has been attempted. This additionally stifles any attempts at formulating new models or improving upon existing ones.

The need is apparent for a practical assessment of existing breathing mode theories and the synthesis of an improved theory, which itself must be validated against experimental observations. The development of such a theory was covered in Part I of this study,**??** and in this manuscript an attempt at experimental validation will be presented. In Section II, the theory of Ref. 3 will be reviewed, as well as several significant aspects of its motivation. Next, the approach for a preliminary validation of this model will be detailed. The results of the ensuing experiment are then presented in Section IV. We then discuss the application of this data to the theoretical model. Finally, in Section VI we summarize this work.

II. Background

The breathing mode has been explored experimentally,[4–6] numerically,[7–10] and theoretically[11–14] with many physical processes attributed to its onset and growth. However, very few of these theories have been experimentally validated, and in fact most are hindered by physical inconsistencies or limited predictive insights. In this section, we examine one of the most prominent descriptions of the breathing mode, the predator-prey model, and then we review a modification of it derived in Part I of this study.

A. Traditional Predator-Prey Model

Fife et al. proposed a Lotka-Volterra, or predator-prey, description of the breathing mode to accompany the results of their 1D hybrid code.[11] In that work, the neutrals were likened to prey and electrons predators, and it was speculated that periodic bursts of ionization followed by neutral droughts were responsible for low-frequency oscillations in Hall thrusters. Using 0D ion and neutral continuity equations, Fife found

$$\omega = \frac{\sqrt{u_i u_n}}{L} \quad , \tag{1}$$

where u_i is the ion velocity, u_n is the neutral velocity, L is a characteristic ionization length, and ω is the breathing frequency. Barral and Ahedo[15] noted that this formulation does not account for the neutral density entering the 0D domain $n_{n,0}$, so accounting for this and other discrepancies, Hara et al.[13] produced the following, where ξ is the ionization rate coefficient and γ is the growth rate defined as the imaginary component of ω:

$$\Re(\omega) = \sqrt{n n_n \xi^2 - \gamma^2} \quad , \tag{2}$$

$$\gamma \equiv \Im(\omega) = -\frac{1}{2}\frac{n_{n,0}}{n_{n,0} - n_n} n\xi \quad . \tag{3}$$

Of note, Eq. (1) typically produces realistic real frequencies when L is comparable to the channel length. Further, Eq. (2) is equivalent to Fife's result in the limit of low growth. However, Eq. (3) is never positive since $n_{n,0} > n_n$ by construction, so the oscillations are always damped and therefore unlikely to exist in a real thruster.

Further work by Barral, Ahedo, and Peradzynski was able to reproduce breathing-like behavior using a quasi-steady 1D fluid model.[15,16] Their results showed standing plasma and neutral density waves reminiscent of the breathing mode, but also a superimposed traveling neutral density wave. Together, this produced a moving ionization front not captured by the traditional predator-prey model. However, the complexity of the model makes it difficult to extract any intuitive physical understanding of the growth mechanism, let alone any simple predictive scaling laws.

B. Two-Zone Predator-Prey Model

In Part I of this study, we proposed a physical process that could be responsible for the breathing mode. Figure 1, repeated from that work, depicts this hypothetical process. In short, we propose that the predator-prey mechanism does exist in the traditional ionization region of the thruster, but it couples to the near-anode region such that the neutral flux leaving that area is modulated. It is shown in Part I that it may be sufficient for the predator-prey model to grow if $n_{n,0}$ fluctuates weakly in phase with n, out of phase with n, or leads n at all. In this "two-zone" predator-prey model, the phase difference between $n_{n,0}$ and n arises from the transit time of electrons from the ionization region to the anode (short) and of neutrals from the anode to the ionization region (long).

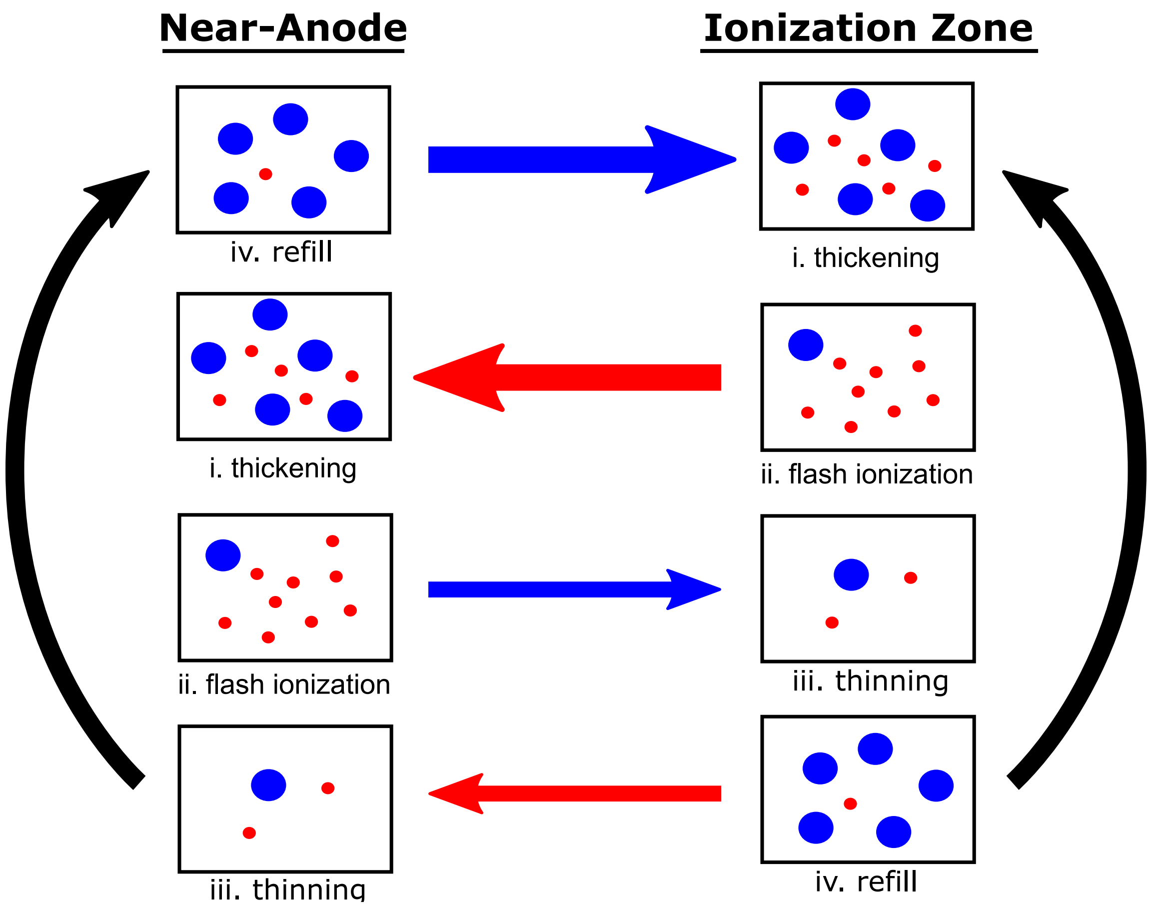

Fig. 1 A diagram of the physical process proposed for the two-zone model, where electrons are shown in red and neutral gas is shown in blue. The righthand cycle represents the typical predator-prey process in the ionization region, and the lefthand cycle represents a similar phenomenon near the anode. The arrows between the two reflect the coupling between the two instabilities.

We modeled this two-zone setup as two coupled pairs of continuity equations: ion and neutral downstream, and electron and neutral upstream. We found that, after applying reasonable assumptions (described completely in Part I), this system is represented by the quartic function

$$\begin{aligned}0 = &\left\{\frac{\eta_1 u_{e,a} {u_n}^2}{\delta^2 L^4}[u_i(3\eta_3 - 1) + u_{e,a}\angle\theta]\right\}\\ -i\omega &\left\{\frac{\eta_1 u_{e,a} u_n}{\delta^2 L^3}[u_n(3\eta_3 - 1) + 2u_i\delta]\right\}\\ -\omega^2 &\left\{\frac{u_n u_{e,a}}{\delta^2 L^2}[(3\eta_3 - 1) + 2\eta_1\delta]\right\}\\ +i\omega^3 &\left\{\frac{1}{\delta L}[2u_{e,a} + u_n\eta_1\delta]\right\}\\ +\omega^4 &\quad ,\end{aligned} \tag{4}$$

where $\delta \equiv \lambda_D/L$, $\eta_1 \equiv n_{n,a}/n_n > 1$, $\eta_2 \equiv n/n_a < 1$, $\eta_3 \equiv n_{n,0}/n_{n,a} > 1$, and $\angle\theta$ is the combined phase lag accrued by electrons and neutrals transiting the channel.

We found that evaluating Eq. (4) numerically for reasonable estimates of the steady-state plasma and neutral parameters, allowing θ and the near-anode electron velocity $u_{e,a}$ as independent variables, predicted vast regions in the parameter space of positive growth and reasonable real frequencies. However, the ambiguity in $u_{e,a}$ in particular cast doubt on the usefulness of this model. In the following section, we will describe an experimental means of attempting to validate this model in an effort to remove these doubts.

III. Methodology

As a preliminary validation of the two-zone model, the independent variables in Part I – the near-anode electron velocity, and the electron and neutral phase delays – must be measured. If the model does not predict growth or plausible real frequencies for realistic steady-state inputs, it cannot be correct. Following that, a numerical solution can be found using measured steady-state parameters, and the observed frequency can be compared to that predicted. To review how this was accomplished, we will briefly discuss the facility, diagnostics, and analytical techniques we employed.

A. Facility

This experiment was conducted in the Large Vacuum Test Facility (LVTF) at the University of Michigan. LVTF is a 6-m diameter and 9-m long vacuum vessel equipped with five cryosails and thirteen cryopumps with LN_2-cooled baffles. The device under test was a 9-kW magnetically-shielded Hall thruster developed jointly by the Jet Propulsion Laboratory, the Air Force Research Laboratory, and the University of Michigan, described in Refs. 17 and 18, and depicted in Fig. 2. It was operated at 300 V and 10 A – a power level within its nominal operating envelope – with 75% nominal magnetic field strength. At this condition, low-frequency oscillations were particularly strong and coherent, exhibiting peak-to-peak discharge current swings of roughly 180% the mean. At this condition, the chamber pressure was about 3 μTorr-Xe.

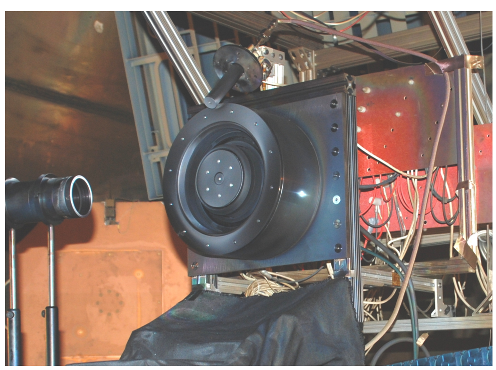

Fig. 2 The 9-kW Hall thruster used in this study, in the test configuration.

B. Diagnostics

This study made use of two major diagnostics: laser-induced fluorescence and near-field electrostatic probing. The former was used to measured the velocity distribution function of both singly-charged and neutral xenon in a time-resolved manner. The latter provided boundary measurements of ion current density and electron temperature. Each will now be briefly described.

1. Laser-induced fluorescence

Laser-induced fluorescence (LIF) is a common diagnostic technique in the electric propulsion field, described thoroughly in the literature.[19] In short, it involves injecting a laser beam into the plasma with a frequency detuned slightly from one that excites a particular metastable transition. Because of the detuning, only particles moving at a specific velocity will be excited by the Doppler-shifted laser light. If the fluorescence spontaneously emitted is measured as a function of detuning frequency, the relative IVDF can be found. In this case, the particle velocity is related to the laser wavelength through the following expression:

$$u = c\frac{\lambda - \lambda_0}{\lambda_0} \quad . \tag{5}$$

The collected fluorescence is generally quite weak compared to the background light emission, so homodyning is performed to elevate the signal from the noise. Since low-frequency oscillations in Hall thrusters are typically $\mathcal{O}$(10 kHz), the laser is modulated at $\mathcal{O}$(1 kHz), and the signal is integrated for $\mathcal{O}$(10 Hz). However, these measurements can also be taken in a time-resolved sense using the thruster discharge current I_d as a trigger signal for a fast sample-and-hold circuit.[20] In this scheme, the sampling gate is progressively delayed within one period of I_d starting from an arbitrary reference phase, allowing the VDF to be measured phase-by-phase.

In this experiment, the Xe II $5d[4]_{7/2}$–$6p[3]_{5/2}$ (834.953 nm) transition was targeted for xenon ions, and the Xe I $6s^2[1/2]^0_1$–$6p^2[3/2]_2$ (834.912 nm) transition for neutral xenon. The setup included a diode laser and tapered amplifier providing the infrared laser light, a wavemeter for measuring the wavelength precisely, and mechanical choppers to modulate the laser. We mounted the thruster on motion stages inside the chamber so that the interrogation volume, approximately 1 mm^3, could be varied relative to the thruster. Specifically, Xe I data was taken 0.92 to 0.26 channel lengths upstream of the exit plane, and Xe II data 0.53 upstream to 1.3 downstream of the exit plane. The fluorescence was filtered ± 4 nm with a set of thin dieletric bandpass filters, transduced with a photomultiplier tube, sampled-and-held with a gated integrator, and homodyned with a lock-in amplifier. This setup is described in depth in Ref. 21. An optogalvanic cell provided a reference for the stationary hyperfine structure of the chosen Xe I transition. Using this information, deconvolution of the measured Xe I spectra to yield VDFs could be accomplished by five-fold gaussian fits rather than the typical intricate filtering techniques.[22]

2. Electrostatic Probing

A planar tungsten electrode with a thin foil guard was used to measure ion current density in the near-field of the thruster, as close as 1.3 channel lengths (z/L=1.3) downstream of the exit plane. At that point, the probe data is coincident with the most downstream LIF measurements. The probe was biased to -40 V, determined by varying the probe bias until current saturation was observed. Collected current was measured with a high-speed digitizer using a 100-Ω shunt. Phase averaging this signal allows the time-resolved ion current density to be measured for a single breathing cycle. As a result, the probe data – as well as all other raw results – are presented in terms of breathing phase (in degrees) rather than time. The probe was strafed in front of the plume using a fast linear motor, minimizing damage to the probe. The discharge current varied by at most 1% during probe injections. Figure 3 is a photograph of the probe tip.

Additionally, the probe was operated like a Langmuir probe to measure electron temperature. In this case, a probe current waveform was measured at each bias and then assembled together after phase-averaging to produce a time-resolved I-V curve for a single breathing cycle. It is typically unfavorable to operate a planar probe facing the plume due to the collection of ram current, but studies have shown that this can have a minimal effect on the measurement of certain plasma properties like electron temperature.[23]

Fig. 3 The tip of the Faraday probe.

C. Boltzmann Analysis

To most thoroughly evaluate the model of Part I, more than just the neutral and ion VDFs must be known. Fortunately, these VDFs can be applied to the 1D Boltzmann equation for ions to infer the ionization frequency, axial electric field strength, and relative plasma density gradient $n\ \partial n/\partial z$ explicitly, and n itself can be determined by integration along ion trajectories using a boundary condition from the electrostatic probe data based on the relation $j_i = enu_i$. Note that this procedure is for the full time-resolved fluid equations, and thus all of these quantities are computed as a function of phase over the course of a breathing cycle. This entire procedure is covered in more depth in Ref. 21 and has heritage in the work of Perez-Luna et al.[24]

A similar process cannot be readily conducted for the neutral population because many complicated kinetic effects contribute to their evolution in the channel and these are difficult to model.[25,26] However, continuity and momentum conservation for the neutral gas can be evaluated throughout the Xe II LIF domain using the Xe I data as an upstream boundary condition. In this way, the only direct neutral measurements yielded by Xe I LIF are u_n and T_n, but indirect information is gained from Xe II LIF.

For the two-zone model, the steady-state parameters required include: u_i, u_n, n, n_n, n_a, and $n_{n,a}$. The first two are direct results of LIF, the next two come from the Xe II Boltzmann analysis, and the last two can be estimated using current and heavy particle continuity (described further in the next section). However, $u_{e,a}$, θ_n, and $\theta_{n,n}$ must also be estimated in some way. The way this was accomplished is described in Section V.

IV. Results

The results of this experiment are presented in this section. First, we provide examples of the discharge current waveform and LIF measurements. Next, we compute the steady-state parameters for the two-zone model. We also present the phase relationships between many of the measured parameters, for use in the next section.

A. Telemetry and Raw LIF Results

Figure 4 shows a sample of the discharge current in the oscillatory operating condition of this study, as well as the frequency spectrum for this sample. The oscillations were vaguely triangular, leading to a defined peak in the power spectrum near 16 kHz, accompanied by several distinguishable harmonics.

Figure 5 shows the phase evolution of the mean neutral and ion velocity at various axial locations. Also included is one cycle of the discharge current signal for reference. Figure 5a shows that the neutral

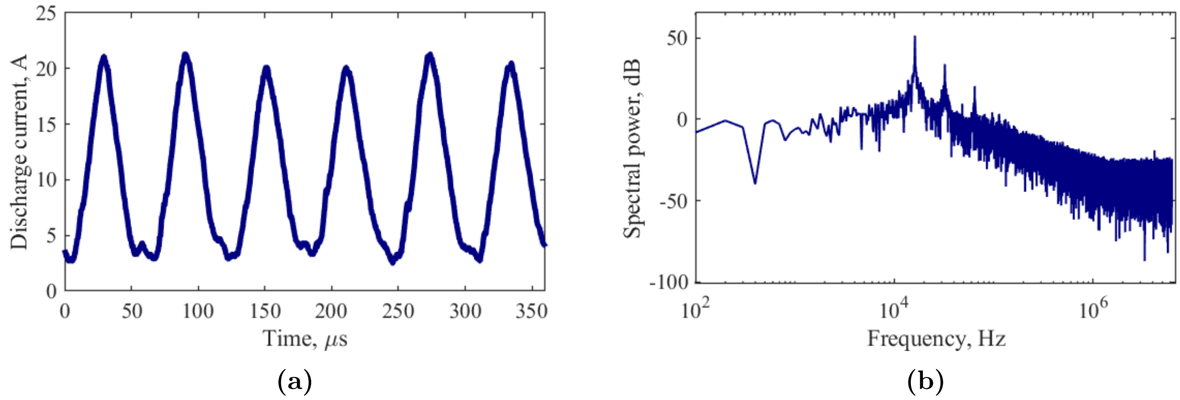

Fig. 4 A sample discharge current waveform (a) and its frequency spectrum (b) for the oscillatory operating condition used in this study.

u_n	310 m/s
u_i	8.5 km/s
u_e	7.6 km/s
n_n	1.4×10^{19} m^{-3}
n	5.4×10^{17} m^{-3}
$n_{n,a}$	2.2×10^{19} m^{-3}
n_a	1.6×10^{17} m^{-3}

Table 1 A summary of the steady-state parameters measured or inferred for use with the two-zone model.

velocity is fairly steady throughout a breathing cycle, while the ion velocity can vary significantly according to Fig. 5b, especially near the exit plane (z/L=0). At this location, the velocity peaks at the minimum in I_d, but the velocity is lowest slightly before the peak in I_d. Farther downstream, the minimum in u_i is nearly at the peak in I_d, and the peak in u_i occurs soon after. In total, this data indicates that the velocity profiles – and thus the moments of u_i that impact the Boltzmann equation – fluctuate measurably throughout a breathing cycle.

B. Steady-State Results

Using the Boltzmann moment analysis, profiles of f_{iz} and E_z were generated as a function of breathing phase. One such set of profiles is shown in Fig. 6a at 278°. Also shown are the mean locations and widths of the ionization and acceleration zones. The mean locations for the ionization and acceleration zones are identified as the position where 50% of ions have been created or 50% of the potential has dropped within the domain, respectively. Similarly, the widths of these a regions are identified as the area around the mean where 90% of ions have been created or 90% of the potential has dropped. We performed this analysis at all measured phases so that the location and extent of the ionization and acceleration zones are known throughout a breathing cycle, as shown in Fig. 6b.

With this information, the steady-state quantities needed to evaluate the two-zone model can be estimated. That is, plasma and neutral properties can be averaged spatially within the ionization-acceleration region and temporally throughout a breathing cycle to yield realistic values with which to evaluate the two-zone model. The results are summarized in Table 1.

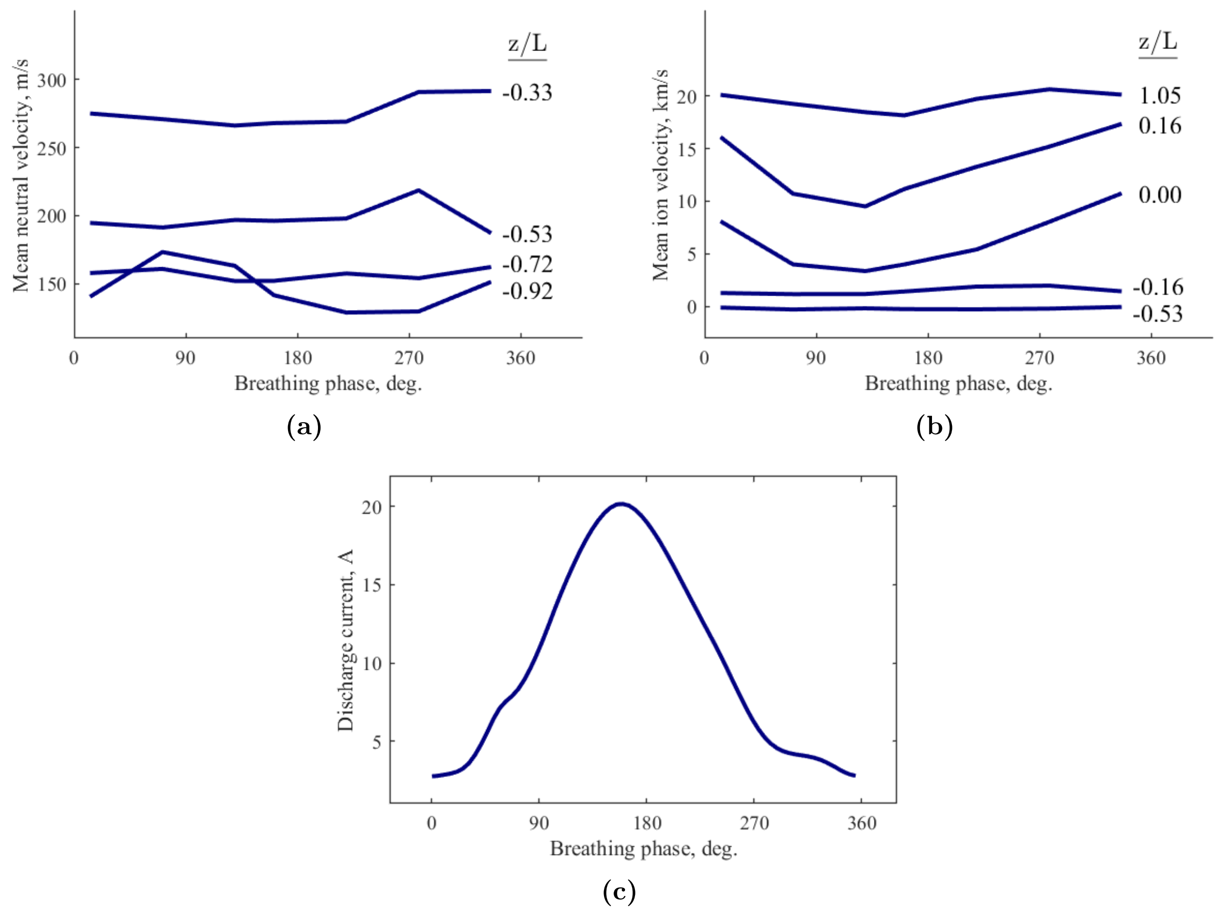

Fig. 5 The variation of the neutral velocity (a), ion velocity (b), and discharge current (c) over breathing phase. For the two velocities, curves are shown for various axial locations to demonstrate the spatial evolution of velocity fluctuations.

Additionally, the phases of many plasma and neutral parameters can be evaluated from the time-resolved data. Figure 7 shows the relative magnitudes and phases of various quantities relative to the discharge current. Many quantities can easily be characterized as in phase ($\theta \approx 0°$), out of phase ($\theta \approx 180°$), leading ($0° < \theta < 180°$), or lagging($0° > \theta > -180°$). In particular, ionization frequency, electron temperature, and axial electric field strength all vary in phase with I_d; ion velocity in the ionization region, and plasma density throughout the ionization-acceleration zone vary out of phase; ion velocity in the acceleration region leads; and neutral density in the ionization region only somewhat lags.

V. Discussion

A. Near-Anode Electron Velocity

Estimating the electron velocity near the anode is still challenging, even given the wealth of information yielded by the Boltzmann analysis. In Part I of this study, we evaluated a wide range of $u_{e,a}$, from 0.1 to 100 km/s. However, the results of this experiment can be used to narrow this region significantly. The major difficulty in specifying $u_{e,a}$ is that the sheath conditions at the anode are unclear. We begin by assuming a negative anode sheath where ions enter at the Bohm speed u_B and

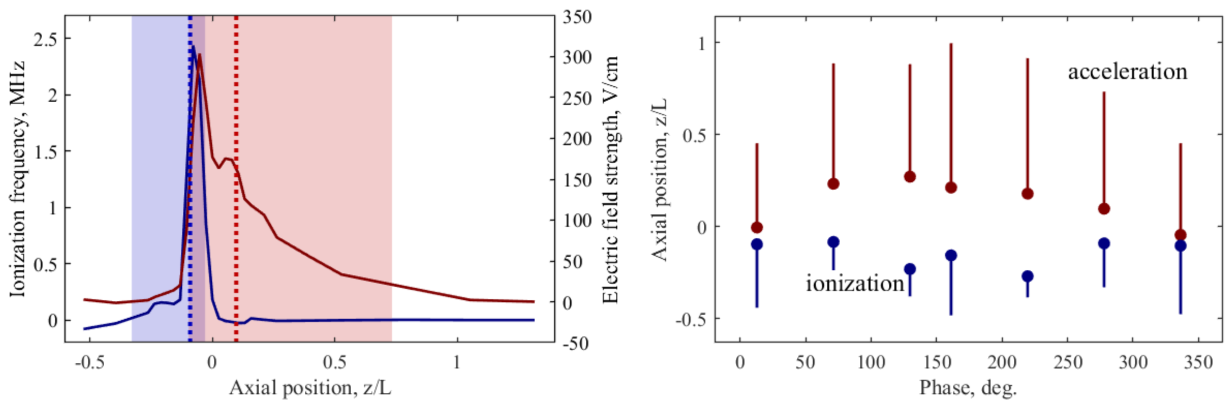

Fig. 6 An example of the ionization and acceleration zones identified using ionization frequency (blue) and electric field strength (red) profiles (a), and the variation in the location and extent of these regions as a function of breathing phase. Only the upstream width for the ionization region is shown, and likewise only the downstream width for the acceleration region is shown.

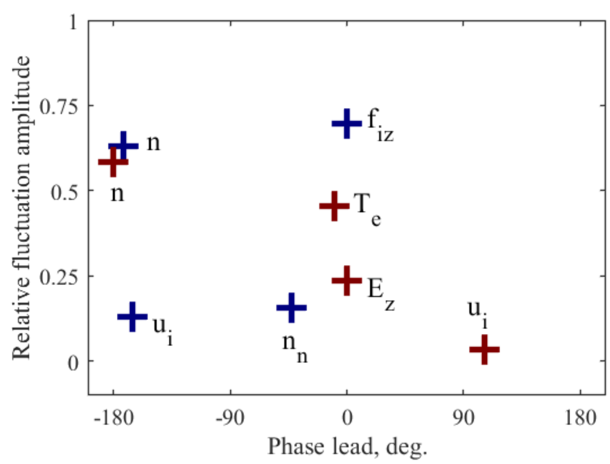

Fig. 7 The relative fluctuation amplitude for various plasma and neutral parameters as a function of phase lead, in the ionization region (blue) and acceleration region (red).

electrons are slightly repelled, as it typical for a thermally non-equilibrium plasma.

First, assuming quasineutrality and a uniform radial distribution of discharge current, the electron velocity can be directly computed anywhere within the LIF domain as

$$u_e = \frac{I_d}{enA} - u_i \quad . \tag{6}$$

The anode presheath – where $u_i = 0$ – was often within the TRLIF spatial domain; u_e at this point is perhaps the simplest estimate of the near-anode electron velocity. In this case, it was found to be 5.7 km/s. At the sheath edge, quasineutrality no longer holds but by assuming a negative collisionless sheath we can apply $n_e \approx 0.61n$ and $u_i \approx u_B$ to Eq. (6) such that $u_{e,a}$=11.6 km/s. Finally, assuming a Maxwellian electron distribution, quasineutrality at the presheath edge, and negligible electron drift compared to T_e, the total sheath potential can be estimated as approximately 11 V. Given that the presheath drop alone should be roughly $2T_e \approx 5$V, this seems reasonable. If the sheath is collisionless, this can then yield a estimate of the electron velocity at the anode: $u_{e,a} = 2143$ km/s. This value is so large because only the few fastest electrons manage to reach the anode surface but must carry more than the discharge current (to compensate for backstreaming ions).

The phase information of Fig. 7 combined with the length data of Fig. 6b also permits an estimate of the average $u_{e,a}$ between the anode and the ionization region as $z_{iz}\omega(\theta_n/2\pi)$, where z_{iz} is the location of the ionization region. This value is found to be about 29 km/s, which is plausible given that $u_{e,a}$ is predicted to be lower than this for a large region (presheath) and much higher than this for a small region (sheath).

In total, we choose to consider $u_{e,a}$ in the presheath, and thus limit the range of possible values from 5.7 to 11.6 km/s.

B. Density Lag

As discussed in Section II, one aspect to validating the two-zone predator-prey model is to experimentally determine θ_n and $\theta_{n,n}$. Rhese are the phase lags accrued by electrons traveling from the ionization region to the anode, and by neutrals traveling oppositely. In analytical terms, this phase lag plays an important role in coupling the downstream and upstream continuity equations. The density phase lags can be determined by Figs. 5 and 7. In the former, u_n can be integrated across the spatial domain to determine an average transit time from the anode to the ionization region. This is found to be 862°, or a lag of 142°. In the latter, the phase lag of n from the ionization region relative to I_d can be used an approximation of the transit phase lag of electrons. From Fig. 7, this lag is roughly 6.5°.

C. Model Validation

Armed with this information, the steady-state parameters of Table 1 can now be used to numerically evaluate the two-zone model. But first it is important to note that the relationships between some quantities are not entirely consistent with the model of Part I. In particular, the near-anode plasma density is less than the downstream density. In the two-zone model, we consider the plasma between the anode and ionization region to be "frozen", such that the electron density must increase near the anode due to ionization. In reality, one would expect the electron density to diminish upstream of the ionization region. In any case, the two-zone model predicts four complex roots for each $u_{e,a}$ used with the given steady-state parameters. In all cases, two roots were damped and two unstable. Of the latter, universally one had a large growth rate but low real frequency, and the other moderate real frequency and growth rate. Figure 8a shows the root loci for the average value of $u_{e,a}$, portraying these trends. The moderate growing root is the one of interest in this case, and Fig. 8b shows the variation of the real and imaginary part with electron velocity. As it depicts, both quantities are certainly $\mathcal{O}(10$ kHz$)$, averaging about 13 kHz over the studied range of $u_{e,a}$, with the growth rate showing more sensitivity to $u_{e,a}$.

The real frequency predicted by the two-zone model is somewhat lower than the experimentally measured value of 16 kHz but is certainly close enough to be physically plausible. The growth rate is nearly identical to the real frequency, which suggests that neither the high nor low growth limits as discussed in Part I are applicable to the thruster operating condition studied here. However, a moderate growth rate suggests to us that the linear analysis of Part I is meaningful, compared to a MHz or GHz growth rate that suggests largely nonlinear development of the instability. In all, this limited experimental validation provides some evidence that the two-zone predator-prey model may be capable of capturing breathing behavior in real thrusters. However, further refinement of the model and/or the experimental validation technique are needed due to the discrepancy in real

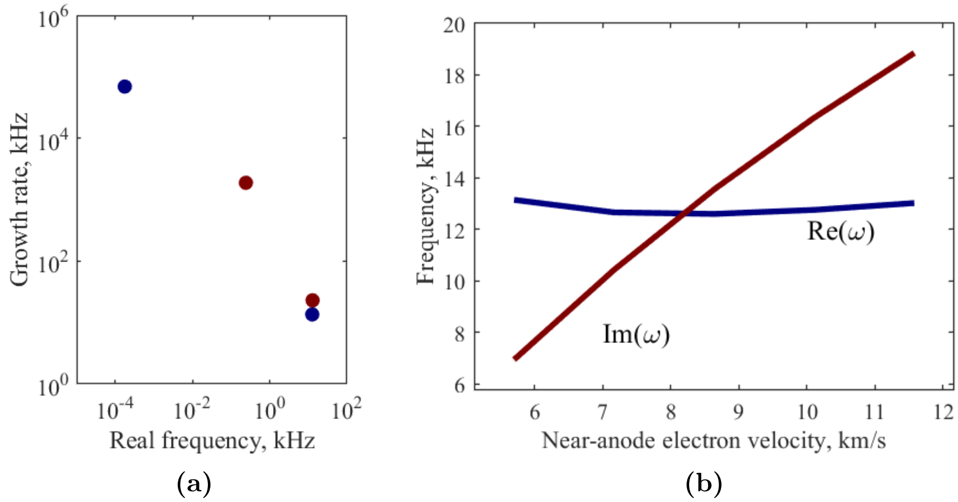

Fig. 8 A sample of root loci for one value of $u_{e,a}$ (a), and the variation in the real frequency (blue) and growth rate (red) with electron velocity (b).

frequency found here.

D. Limitations

Although in this study we have presented experimental evidence that suggests the two-zone model is accurate, there are several notable limitations in this validation effort. First, we have not presented any circumstantial evidence that the two-zone predator-prey process actually exists. That is, we have shown that the results of our analytical model are roughly in agreement with experimental observations, but we have not shown that the model is physically actualized. For example, it is not clear that there is significant ionization near the anode, let alone enough ionization to meaningfully modulate the upstream neutral flow.

Second, the steady-state parameters we used to evaluate the two-zone model numerically rely on many assumptions that are only weakly justified in this work. For instance, 1D current and heavy particle continuity is assumed to allow estimates of steady-state densities given the available LIF data, but radial particle fluxes may exist.

Finally, even though we have performed a preliminary validation of the two-zone model, we have yet to assess its scaling predictions and its ability to capture trends with high-level operating parameters. That is, we have not shown that the two-zone model can predict variations in breathing frequency or intensity, nor have we shown that it accurately reflects changes in these properties with discharge voltage, propellant mass flow, and other operating parameters. Such a study is not outside of the capabilities of the diagnostic and analytical techniques presented in this work, though, and thus it is reserved for future investigation.

VI. Conclusions

In summary, this study is a continuation of Part I (Ref. 3) in which a new formulation of the predator-prey model of the breathing mode was presented. After reviewing that model, a means of preliminary validation was outlined in which laser-induced fluorescence would provide the time-resolved plasma and neutral parameters required to numerically assess the model. With this data, steady-state velocities and densities in the ionization-acceleration region and near-anode region were estimated. Further, several independent variables from Part I were experimentally clarified. Applying these measurements to the model, a real frequency and positive growth rate both near 13 kHz was calculated, which suggests that the model is able to capture breathing behavior to some extent when compared to the experimental value of 16 kHz. This provides a new physical explanation for the breathing mode that was lacking in the traditional predator-prey model.

References

[1] Lev, D., Myers, R., Lemmer, K., Kolbeck, J., Keidar, M., Koizumi, H., Liang, H., Yu, D., Schönherr, T., Gonzalez, J., Choe, W., Albertoni, R., Hoskins, A., Yan, S., Hart, W., R Hofer, R., Funaki, I., Lovtsov, A., Polzin, K., and Duchemin, O., "The Technological and Commercial Expansion of Electric Propulsion in the Past 24 Years," *35th International Electric Propulsion Conference*, Atlanta, GA, Oct. 2017.

[2] Oh, D. Y., Snyder, J. S., Goebel, D. M., Hofer, R. R., and Randolph, T. M., "Solar Electric Propulsion for Discovery-Class Missions," *Journal of Spacecraft and Rockets*, Vol. 51, No. 6, 2014, pp. 1822–1835.

[3] Dale, E. T. and Jorns, B. A., "Two-zone Hall thruster breathing mode mechanism, Part I: Theory," *36th International Electric Propulsion Conference*, University of Vienna, Austria, Sept. 2019.

[4] Chesta, E., Lam, C. M., Meezan, N. B., Schmidt, D. P., and Cappelli, M. A., "A characterization of plasma fluctuations within a Hall discharge," *IEEE Transactions on Plasma Science*, Vol. 29, No. 4, Aug. 2001, pp. 582–591.

[5] McDonald, M. S., Bellant, C. K., Pierre, B. A. S., and Gallimore, A. D., "Measurement of cross-field electron current in a Hall thruster due to rotating spoke instabilities," *47th AIAA/ASME/SAE/ASEE Joint Propulsion Conference & Exhibit*, American Institute of Aeronautics and Astronautics, San Diego, CA, 2011.

[6] Sekerak, M., McDonald, M., Hofer, R., and Gallimore, A., "Hall thruster plume measurements from High-speed Dual Langmuir Probes with Ion Saturation Reference," *2013 IEEE Aerospace Conference*, March 2013, pp. 1–16.

[7] Boeuf, J. P. and Garrigues, L., "Low frequency oscillations in a stationary plasma thruster," *Journal of Applied Physics*, Vol. 84, No. 7, Oct. 1998, pp. 3541–3554.

[8] Parra, F. I., Ahedo, E., Fife, J. M., and Martínez-Sánchez, M., "A two-dimensional hybrid model of the Hall thruster discharge," *Journal of Applied Physics*, Vol. 100, No. 2, July 2006, pp. 023304.

[9] Adam, J. C., Héron, A., and Laval, G., "Study of stationary plasma thrusters using two-dimensional fully kinetic simulations," *Physics of Plasmas*, Vol. 11, No. 1, Jan. 2004, pp. 295–305.

[10] Hara, K., Boyd, I. D., and Kolobov, V. I., "One-dimensional hybrid-direct kinetic simulation of the discharge plasma in a Hall thruster," *Physics of Plasmas*, Vol. 19, No. 11, Nov. 2012, pp. 113508.

[11] Fife, J., Martinez-Sanchez, M., and Szabo, J., "A numerical study of low-frequency discharge oscillations in Hall thrusters," *33rd AIAA/ASME/SAE/ASEE Joint Propulsion Conference & Exhibit*, American Institute of Aeronautics and Astronautics, July 1997.

[12] Chable, S. and Rogier, F., "Numerical investigation and modeling of stationary plasma thruster low frequency oscillations," *Physics of Plasmas*, Vol. 12, No. 3, Feb. 2005.

[13] Hara, K., Sekerak, M. J., Boyd, I. D., and Gallimore, A. D., "Perturbation analysis of ionization oscillations in Hall effect thrusters," *Physics of Plasmas (1994-present)*, Vol. 21, No. 12, Dec. 2014.

[14] Koshkarov, O., Smolyakov, A. I., Romadanov, I. V., Chapurin, O., Umansky, M. V., Raitses, Y., and Kaganovich, I. D., "Current flow instability and nonlinear structures in dissipative two-fluid plasmas," *Physics of Plasmas*, Vol. 25, No. 1, Jan. 2018, pp. 011604.

[15] Barral, S. and Ahedo, E., "Low-frequency model of breathing oscillations in Hall discharges," *Physical Review E*, Vol. 79, No. 4, April 2009.

[16] Barral, S. and Peradzyński, Z., "Ionization oscillations in Hall accelerators," *Physics of Plasmas (1994-present)*, Vol. 17, No. 1, Jan. 2010.

[17] Hofer, R., Cusson, S., Lobbia, R., and Gallimore, A., "The H9 Magnetically Shielded Hall Thruster," *35th International Electric Propulsion Conference*, Vol. IEPC- 2017- 232, 2017.

[18] Cusson, S., Hofer, R., Lobbia, R., Jorns, B., and Gallimore, A., "Performance of the H9 Magnetically Shielded Hall Thrusters," *35th International Electric Propulsion Conference*, Vol. IEPC-2017-239, 2017.

[19] Mazouffre, S., "Laser-induced fluorescence diagnostics of the cross-field discharge of Hall thrusters," *Plasma Sources Science and Technology*, Vol. 22, No. 1, 2013, pp. 013001.

[20] MacDonald, N. A., Cappelli, M. A., and Hargus, W. A., "Time-synchronized continuous wave laser-induced fluorescence on an oscillatory xenon discharge," *Review of Scientific Instruments*, Vol. 83, No. 11, Nov. 2012, pp. 113506.

[21] Dale, E., Gallimore, A., and Lobbia, R., "Time-resolved internal Hall thruster plasma measurements using a high-speed Langmuir probe," Phoenix, AZ, Dec. 2016.

[22] Smith, T. B., *Deconvolution of ion velocity distributions from laser-induced fluorescence spectra of xenon electrostatic thruster plumes*, Ph.D. thesis, University of Michigan, Ann Arbor, MI, 2003.

[23] Sheridan, T. E. and Goree, J., "Langmuir-probe characteristic in the presence of drifting electrons," *Physical Review E*, Vol. 50, No. 4, Oct. 1994, pp. 2991–2996.

[24] Perez-Luna, J., Hagelaar, G. J. M., Garrigues, L., and Boeuf, J. P., "Method to obtain the electric field and the ionization frequency from laser induced fluorescence measurements," *Plasma Sources Science and Technology*, Vol. 18, No. 3, 2009, pp. 034008.

[25] Huang, W., Gallimore, A. D., and Hofer, R. R., "Neutral Flow Evolution in a Six-Kilowatt Hall Thruster," *Journal of Propulsion and Power*, Vol. 27, No. 3, May 2011, pp. 553–563.

[26] Mazouffre, S., Bourgeois, G., Garrigues, L., and Pawelec, E., "A comprehensive study on the atom flow in the cross-field discharge of a Hall thruster," *Journal of Physics D: Applied Physics*, Vol. 44, No. 10, 2011, pp. 105203.